UDC 621.313 https://doi.org/10.20998/2074-272X.2022.1.04

L. Moussaoui

Performance enhancement of direct torque control induction motor drive using space vector modulation strategy

Purpose. *The main objective of this work is to demonstrate the advantages brought by the use of space vector modulation technique in the direct torque control of the induction motor. To achieve this purpose, two different direct torque control approaches (with space vector modulation) are proposed and studied from a comparative aspect with each other and with the conventional direct torque control.* ***The novelty*** *of this work consists in the employment of an Integral-Proportional (IP) speed controller in the two proposed direct torque control approaches and a more in-depth evaluation for their performance mainly the switching frequency of inverter semiconductor components and motor torque ripples.* ***Methods.*** *Two different direct torque control approaches that use the space vector modulation strategy and/or fuzzy-logic control, are described in detail and simulated with IP speed controller. The simulation experiments are carried out using Matlab/Simulink software and/or fuzzy-logic tools.* ***Results. Practical value.*** *Comparison results show that the two proposed direct torque control structures (with space vector modulation) exhibit a large reduction in torque ripples and can also avoid random variation problem of switching frequency (over a wide range of speed or torque control). On the other hand, the use of IP speed regulator ensured good dynamic performance for the drive system as well as considerably minimized peak overshoot in the speed response. Practically all of these benefits are achieved while retaining the simplicity and the best dynamic characteristics of the classical direct torque control, especially with the modified direct torque control approach in which the design or implementation requires minimal computational effort.* References 23, tables 4, figures 17.
Key words: **induction motor drive, direct torque control, voltage source inverter, space vector modulation, IP controller, fuzzy control.**

Мета. *Основна мета даної роботи – продемонструвати переваги використання методу модуляції просторового вектора при прямому регулюванні крутного моменту асинхронного двигуна. Для досягнення цієї мети запропоновано два різних підходи до прямого управління крутним моментом (з модуляцією просторового вектора), які досліджуються з порівняльної точки зору одного з іншим, а також зі звичайним прямим керуванням крутним моментом.* ***Новизна*** *роботи полягає у використанні інтегрально-пропорційного (ІП) регулятора швидкості в двох запропонованих підходах до прямого регулювання крутного моменту та більш поглибленій оцінці їх ефективності, головним чином, частоти перемикань напівпровідникових компонентів інвертора та пульсації крутного моменту двигуна.* ***Методи***. *Два різних підходи до прямого керування крутним моментом, які використовують стратегію модуляції просторового вектора та/або керування нечіткою логікою, детально описані та змодельовані за допомогою ІП-регулятора швидкості. Обчислювальні експерименти проводяться з використанням програмного забезпечення Matlab/Simulink та/або інструментів нечіткої логіки.* ***Результати***. ***Практична цінність***. *Результати порівняння показують, що дві запропоновані структури прямого керування крутним моментом (з модуляцією просторового вектора) демонструють значне зниження пульсації крутного моменту, а також можуть уникнути проблеми випадкових змін частоти перемикання (у широкому діапазоні регулювання швидкості або крутного моменту). З іншого боку, використання ІП-регулятора швидкості забезпечило хороші динамічні характеристики для приводної системи, а також значно знизило пікове перевищення швидкості. Практично всі ці переваги досягаються при збереженні простоти та найкращих динамічних характеристик класичного прямого керування крутним моментом, особливо з модифікованим підходом прямого керування крутним моментом, при якому проектування або впровадження вимагає мінімальних обчислювальних витрат*. Бібл. 23, табл. 4, рис. 17.
Ключові слова: **електропривод з асинхронним двигуном, пряме керування крутним моментом, інвертор джерела напруги, модуляція просторового вектора, ІП-регулятор, нечітке керування.**

Introduction. Three-phase induction motors have been widely used in industrial applications due to their low maintenance, high robustness, simple structure and high efficiency. In fact, in high performance applications such as motion control of an induction motor (IM), it is generally desirable that motor can provide a good dynamic torque response as it's in DC motor drive. In order to achieve this objective, many researchers have focused on developing several control algorithms. Recently, an innovative control method, called Direct Torque Control (DTC) is introduced because of its capability to produce a fast torque control for the IM without to use much on-line computation as it's in field oriented control [1-13].

Indeed, the main advantages offered by DTC are:

- Excellent torque dynamic with minimal response time;
- robustness against rotor parameters variation;
- decoupled control between the torque and stator flux;
- no need of voltage modulator;
- control method without inherent speed sensor.

These merits are counterbalanced by some drawbacks like:

- Possible problems either when starting the machine, or running at low speed or changing the load torque;
- requirement for torque and flux estimation which includes machine parameters identification;
- inherent ripples in the torque and stator flux;
- greater harmonic distortion in stator voltages and waveforms of currents;
- inverter switching states remain unchanged in a number of sample cycles. Thus, the switching frequency is not constant and inverter power components capacity will not be wholly utilized;
- acoustical noise produced because of random inverter switching frequency variation [1-4], [14-18].

To overcome these problems, a variety of techniques with different concepts are described in the literature. Some of diverse proposed solutions include DTC with; space vector modulation, various power converter topologies such as: multi-level inverter and matrix converter, sensorless

control methods, optimal stator flux estimation for high speed operation and artificial intelligence techniques (fuzzy or neuro controllers) [1, 2, 4-8, 14-21]. These methods achieve certain improvements such as reduction of torque ripples and fixed switching frequency operation. However, control system complexity is greatly increased.

The goal of the paper. In order to solve problems, of ripples in both electromagnetic torque and stator flux and of random variation of inverter switching frequency, we have proposed and study in this work two different Direct Torque Control approaches making use of Space Vector Modulation technique (DTC-SVM) and/or fuzzy logic control.

Practically, fuzzy logic is considered as an interesting alternative approach for its advantages such as: analysis close to exigencies of users, ability of nonlinear systems control, best dynamic performances and inherent quality of robustness. On the other hand, SVM strategy uses a digital algorithm to obtain an appropriate switching states sequence for Voltage Source Inverter (VSI) control. Thus, inverter can generate an output voltage vector which is closest to its reference voltage vector, with a previously imposed switching frequency. Also, in conventional DTC a single voltage vector is applied throughout the sample time. Therefore, for small torque errors, motor torque may exceed its upper or lower limit. Instead, with SVM strategy, which uses more than one vector during sample period, torque ripples can be reduced.

Subject of investigations. First proposed DTC-SVM approach, called Direct Fuzzy Torque Control (DFTC), is introduced with the aim of reducing ripples of electromagnetic torque and stator flux and improving stator currents waveform. The so-called DFTC uses both SVM technique and hysteresis comparators. In this approach, a look-up table decides angle choice of voltage vector applied to the motor, while an estimator based on fuzzy logic calculates the amplitude of this vector. Thus, reference voltage vector will be synthesized using the space vector modulation.

The second DTC-SVM approach, named Modified Direct Torque Control (MDTC), uses an efficient algorithm, based on direct stator flux control, to independently control amplitude and position of reference stator flux vector of the IM. In fact, the proposed algorithm of MDTC structure is designed to calculate reference voltage vector amplitude leading to an optimal torque and stator flux control.

Performances of these two DTC-SVM approaches are demonstrated by simulation using Matlab/Simulink software and/or fuzzy logic tools. Simulation results are compared to those of classical DTC with the use of an IP controller in all studied DTC structures. Systems performances evaluation is carried out mainly based on; inverter switching frequency, dynamic responses of torque/speed and flux, ripples content in torque and stator flux and distortion of stator currents or stator voltages. The comparison results illustrate clearly the effectiveness and superiority of the proposed DTC-SVM approaches over conventional DTC.

Modeling of the induction motor and voltage source inverter. In order to properly design or simulate a control structure, mathematical model of the latter must be considered [4, 11, 12, 16]. So, under the usual assumption of no hysteresis, no eddy currents and no space harmonics, electrical model of IM can be expressed (in a stationary reference frame) by the following nonlinear equations:

$$\begin{cases} \overrightarrow{V_S} = R_S \cdot \overrightarrow{i_S} + \dfrac{\mathrm{d}\overrightarrow{\phi_S}}{\mathrm{d}t}; \\ \overrightarrow{V_r} = R_r \cdot \overrightarrow{i_r} + \dfrac{\mathrm{d}\overrightarrow{\phi_r}}{\mathrm{d}t} - j \cdot \omega \cdot \overrightarrow{\phi_r}; \end{cases} \quad (1)$$

$$\begin{cases} \overrightarrow{\phi_S} = L_S \cdot \overrightarrow{i_S} + L_m \cdot \overrightarrow{i_r}; \\ \overrightarrow{\phi_r} = L_r \cdot \overrightarrow{i_r} + L_m \cdot \overrightarrow{i_S}, \end{cases} \quad (2)$$

where R_S, L_S, R_r, L_r are the resistances and cyclic inductances of stator and rotor respectively; $\overrightarrow{V_S}$, $\overrightarrow{i_S}$, $\overrightarrow{\phi_S}$, $\overrightarrow{V_r}$, $\overrightarrow{i_r}$, $\overrightarrow{\phi_r}$ are the voltage, current and flux vectors of stator and rotor respectively; L_m, ω are the mutual inductance and electric motor speed (or rotor frequency).

The electromagnetic torque is expressed as a function of the stator and rotor fluxes

$$\Gamma_e = \frac{3}{2} \cdot p \cdot \frac{L_m}{\sigma \cdot L_S \cdot L_r} \cdot \left(\overrightarrow{\phi_S} \times \overrightarrow{\phi_r} \right), \quad (3)$$

where p is the number of pairs of poles and σ ($\sigma = 1 - L_m^2 / L_S \cdot L_r$) is the motor dispersion coefficient.

Elimination of $\overrightarrow{i_S}$ and $\overrightarrow{i_r}$ from (1) and (2), gives the state form model of the induction machine with the stator and rotor fluxes as state variables and τ_S ($\tau_S = L_S/R_S$), τ_r ($\tau_r = L_r/R_r$) are the stator and rotor time constants respectively

$$\begin{bmatrix} \dfrac{\mathrm{d}\overrightarrow{\phi_S}}{\mathrm{d}t} \\ \dfrac{\mathrm{d}\overrightarrow{\phi_r}}{\mathrm{d}t} \end{bmatrix} = \begin{bmatrix} -\dfrac{1}{\sigma \cdot \tau_S} & \dfrac{L_m}{\sigma \cdot \tau_S \cdot L_r} \\ \dfrac{L_m}{\sigma \cdot \tau_r \cdot L_S} & j \cdot \omega - \dfrac{1}{\sigma \cdot \tau_r} \end{bmatrix} \cdot \begin{bmatrix} \overrightarrow{\phi_S} \\ \overrightarrow{\phi_r} \end{bmatrix} + \begin{bmatrix} 1 \\ 0 \end{bmatrix} \cdot \overrightarrow{V_S}, \quad (4)$$

The mechanical mode, associated with the rotor motion, is described by:

$$J \cdot \frac{\mathrm{d}\Omega}{\mathrm{d}t} + f \cdot \Omega = \Gamma_e - \Gamma_r(\Omega), \quad (5)$$

where Γ_r and Γ_e are respectively the load torque and electromagnetic torque developed by the machine; J, f and Ω are the respectively inertia, friction motor coefficient and mechanical rotation speed ($\Omega = \omega / p$).

Figure 1 reveals the diagram of a typical three-phase VSI [4, 9, 10, 13, 22]. Here semiconductors are considered as ideal switches and S_a, S_b, S_c are switching states of each leg of this inverter. Relationships between switching states and phase output voltages (v_{an}, v_{an}, v_{cn}) can be expressed as below:

$$\begin{bmatrix} v_{an} \\ v_{bn} \\ v_{cn} \end{bmatrix} = \frac{V_{dc}}{3} \begin{bmatrix} 2 & -1 & -1 \\ -1 & 2 & -1 \\ -1 & -1 & 2 \end{bmatrix} \cdot \begin{bmatrix} S_a \\ S_b \\ S_c \end{bmatrix}, \quad (6)$$

where n is the neutral point of inverter load.

As it is well known, two-level voltage inverter has in principle eight possible combinations for its switching states. Where two of these combinations are termed as zero vectors and they are designated homogeneously as state 0 ($\overrightarrow{V_0} = \overrightarrow{V_7} = \vec{0}$), as their effects are equal.

The remaining six states represent stationary vectors in the complex α–β plane (Fig. 2).

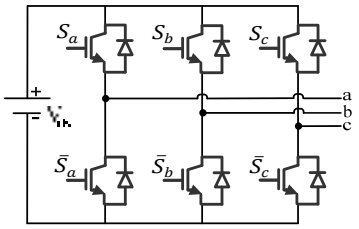

Fig. 1. Schematic diagram of a two-level VSI

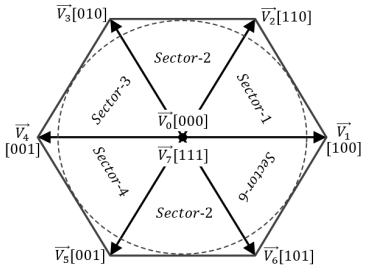

Fig. 2. Illustration of VSI state vectors in the α–β plane

These six active state vectors can be expressed as follows:

$$\overrightarrow{V_k} = \frac{2}{3} \cdot V_{dc} \cdot e^{j \cdot (k-1) \cdot \frac{\pi}{3}}, \quad k = 1, 2, ...6, \tag{7}$$

where V_{dc} is the DC-link voltage.

This equation shows that the amplitude of each active vector is $(2/3) \cdot V_{dc}$ with a deviation angle of $\pi/3$ between the different active vectors, thus building a regular hexagon with two zero vectors which are located at its origin (Fig. 2).

Basic concepts of DTC. The basic configuration of conventional DTC, proposed by Takahashi, is shown in Fig. 3.

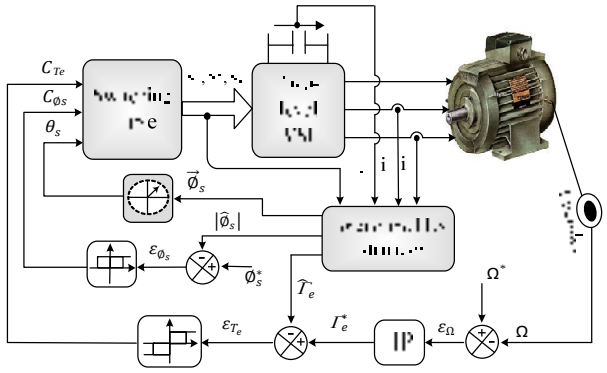

Fig. 3. Block diagram of the classical DTC

It consists of a pair of hysteresis comparators, torque and flux estimators, voltage vector selector and a two-level VSI. The fundamental idea of DTC is to choose the most appropriate voltage vector which allows simultaneous and independent control of stator flux and electromagnetic torque, thus ensuring decoupled control for these two machine quantities. In fact, the performance of this control technique depends directly on the estimation of torque and stator flux so that an incorrect estimation will result in a wrong selection of inverter state vectors [1-8, 14, 16-18, 20, 21, 23].

Mainly in DTC technique, torque and stator flux estimation can be done by means of measurement; of two or three different phase currents (i_{Sa}, i_{Sb}, i_{Sc}) and of DC-link voltage. In fact, estimation procedure is carried out using the following equations:

$$\begin{cases} i_{S\alpha} = i_{Sa}; \\ i_{S\beta} = \frac{1}{\sqrt{3}} \cdot (i_{Sb} - i_{Sc}); \end{cases} \tag{8}$$

$$\begin{cases} v_{S\alpha} = \frac{2}{3} \cdot V_{dc} \cdot \left(S_a - \frac{S_b + S_c}{2} \right); \\ v_{S\beta} = \frac{1}{\sqrt{3}} \cdot V_{dc} \cdot (S_b - S_c). \end{cases} \tag{9}$$

Estimated stator flux is then given by:

$$\begin{cases} \hat{\phi}_{S\alpha} = \int_0^t (v_{S\alpha} - R_S \cdot i_{S\alpha}) dt; \\ \hat{\phi}_{S\beta} = \int_0^t (v_{S\beta} - R_S \cdot i_{S\beta}) dt, \end{cases} \tag{10}$$

where $v_{s\alpha,\beta}$, $i_{s\alpha,\beta}$ and $\hat{\phi}_{S\alpha,\beta}$ are the two α–β components of stator voltage, current and estimated flux respectively.

The electromagnetic torque is estimated on-line by knowledge of instantaneous values of direct and quadratic components of the stator flux and stator current:

$$\hat{\Gamma}_e = \frac{3}{2} \cdot p \cdot \left(\hat{\phi}_{S\alpha} \cdot i_{S\beta} - \hat{\phi}_{S\beta} \cdot i_{S\alpha} \right). \tag{11}$$

As it can be seen in Fig. 3, there are two different loops corresponding to magnitude control of stator flux and electromagnetic torque. Thus reference values of torque and stator flux are compared with their estimated values and resulting errors are then used as inputs into two hysteresis blocks with three-level and two-level respectively. Outputs of these latter blocks, giving torque and stator flux correction states, as well as stator flux position, are used as inputs in the look-up table of Takahashi, as it's depicted in Table 1.

Table 1

Switching table of the classical DTC

Flux sector		1	2	3	4	5	6
$C_{\phi s} = 1$	$C_{Te}=1$	$V2_{(110)}$	$V3_{(010)}$	$V4_{(011)}$	$V5_{(001)}$	$V6_{(101)}$	$V1_{(100)}$
	$C_{Te}=0$	$V7_{(111)}$	$V0_{(000)}$	$V7_{(111)}$	$V0_{(000)}$	$V7_{(111)}$	$V0_{(000)}$
	$C_{Te}=-1$	$V6_{(101)}$	$V1_{(100)}$	$V2_{(110)}$	$V3_{(010)}$	$V4_{(011)}$	$V5_{(001)}$
$C_{\phi s} = 0$	$C_{Te}=1$	$V3_{(010)}$	$V4_{(011)}$	$V5_{(001)}$	$V6_{(101)}$	$V1_{(100)}$	$V2_{(110)}$
	$C_{Te}=0$	$V0_{(000)}$	$V7_{(111)}$	$V0_{(000)}$	$V7_{(111)}$	$V0_{(000)}$	$V7_{(111)}$
	$C_{Te}=-1$	$V5_{(001)}$	$V6_{(101)}$	$V1_{(100)}$	$V2_{(110)}$	$V3_{(010)}$	$V4_{(011)}$

This switching table gives the inverter state vectors which will be applied, to the IM, during a sample period. Such that torque and stator flux errors tend to be restricted in their respective hysteresis bands [1, 4, 8, 15, 16, 19, 20, 23].

In order to reduce motor speed response time and cancel its static error while maintaining system stability, a Proportional-Integral (PI) corrector is generally used. In this work, an Integral-Proportional (IP) controller is applied for IM speed control, because of its various advantages such as good rejection of perturbations (zero static error) and overshoot restriction are obtained by a judicious tuning of its parameters.

The speed control block diagram, including the IP regulator, is illustrated in the Fig. 4, where the integral

part is in the feedforward path and the proportional part is in the feedback path.

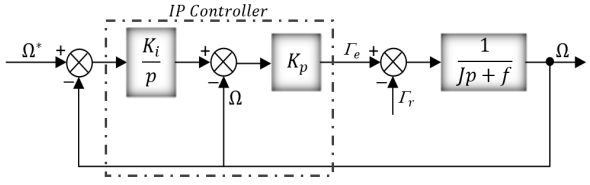

Fig. 4. Speed control loop with IP regulator

Direct Fuzzy Torque Control (DFTC). The corresponding structure of DFTC employs space vector modulation strategy as shown in Fig. 5. In this case, flux and torque errors are used as two inputs either to fuzzy logic estimator of reference voltage vector amplitude $|\overrightarrow{V_S^*}|$ or to hysteresis comparators that deliver errors levels ($C_{\Gamma e}$, $C_{\phi S}$) which are used for determining $\overrightarrow{V_S^*}$ position (via a lookup table).

Unlike the conventional DTC technique, where the applied voltage vector has constant amplitude even if the motor torque is outside its hysteresis band, DFTC structure allows the calculation of an optimum voltage, which will be used in the control of IM, according to the states of torque and stator flux in relation to their desired values. Thus providing a fast and accurate control of the electromagnetic torque. In fact, this optimal voltage vector is synthesized using SVM block which generates the most appropriate switching states to the inverter [3, 14, 16, 23].

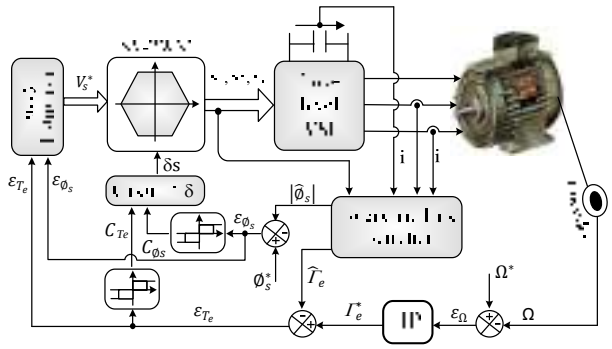

Fig. 5. Block diagram of the proposed DFTC approach

In this DTC approach, the reference voltage vector position relative to the stator flux vector must be chosen so as to maintain the stator flux and electromagnetic torque in an optimal error band around their respective reference values. Indeed, the position of this voltage vector (δ_S) is obtained by adding an angle (δ) to the position of stator flux (θ_S) such as:

$$\delta_S = \delta + \theta_S \,. \qquad (12)$$

The angle δ is selected based on hysteresis comparators output values as depicted in Table 2. It should be noted here, that both hysteresis regulators of torque and stator flux are three levels comparators.

Table 2

Selection of the stator voltage vector position

$C_{\Gamma e}$	–1			0			1		
$C_{\phi S}$	–1	0	1	–1	0	1	–1	0	1
δ	$-\frac{2\pi}{3}$	$+\pi$	$+\frac{2\pi}{3}$	$-\frac{\pi}{2}$	$+\frac{\pi}{2}$	$+\frac{\pi}{2}$	$-\frac{\pi}{3}$	0	$+\frac{\pi}{3}$

Also, reference voltage vector amplitude must be chosen so as to reduce flux and torque errors. Thus, a fuzzy logic estimator (FLE) is designed to generate the most appropriate amplitude of the reference voltage vector. Proposed estimator block diagram, that combines «fuzzification – rules base – defuzzification» modules, is given in the Fig. 6.

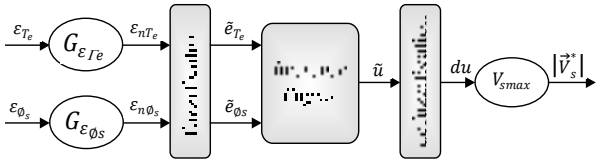

Fig. 6. Proposed fuzzy estimator for voltage vector amplitude estimation

In fuzzification module, inputs are crisp physical signals ($\varepsilon_{n\Gamma e}$, $\varepsilon_{n\phi s}$) of real process and outputs are fuzzy subsets consisting of intervals and membership functions ($\tilde{e}_{\Gamma e}, \tilde{e}_{\phi s}$). These outputs will be inputs for the next module, fuzzy logic IF-THEN rules base of control, which requires fuzzy-subset inputs in order to be compatible with fuzzy logic rules [15, 18, 19, 22].

The general procedure in designing a fuzzy logic rules base includes the following:

- defining process states and control variables;
- determining input variables to inference engine block;
- forming a fuzzy logic IF-THEN rules base (determined input variables in previous step will be used in rules base design);
- establishing a fuzzy logic inference engine.

In fact, this latter phase explains how FLE decides on an optimal reference voltage vector amplitude ($|\overrightarrow{V_S^*}|$) based on the control rules and linguistic terms. In general, inference systems have two types, namely Mandani and Takagi-sugeno [18, 21, 22]. Mandani method is used in this study because of its simple structure and design. Fuzzy rules consist of IF-THEN linguistic terms, and output membership functions are operated by fuzzy rules that are related to both inputs ($\varepsilon_{\Gamma e}$, $\varepsilon_{\phi s}$) and output ($|\overrightarrow{V_S^*}|$). Inference engine block, based on input fuzzy variables uses forty-nine IF-THEN rules, where AND method corresponds to minimum fuzzy inputs, in order to obtain final output fuzzy sets as shown in Table 3. These rules are setting in turn to take maximal amplitude for voltage vector, when torque is outside its error band. Otherwise, zero amplitude is assigned to this voltage vector.

Table 3

Complete rules base for the proposed FLE

	$\tilde{e}_{\Gamma e}$						
$\tilde{e}_{\phi s}$	NH	NM	NS	ZE	PS	PM	PH
NH	PH	PM	PS	PS	PS	PM	PH
NM	PH	PM	PS	PS	PS	PM	PH
NS	PH	PM	PS	ZE	PS	PM	PH
ZE	PH	PM	PS	ZE	PS	PM	PH
PS	PH	PM	PS	ZE	PS	PM	PH
PM	PH	PM	PS	PS	PS	PM	PH
PH	PH	PM	PS	PS	PS	PM	PH
NH – negative high, NM – negative medium, NS – negative small, ZE – zero, PS – positive small, PM – positive medium, PH – positive high							

In this work the fuzzification and defuzzification processes are carried out using asymmetrical triangular membership functions (so that computation complexity can be reduced) as shown in Fig. 7, where each of input variables ($\varepsilon_{n\Gamma e}$, $\varepsilon_{n\phi s}$) is mapped into seven different linguistic values. Mapping relationship between the inputs and output variables of FLE is also given in Fig. 8.

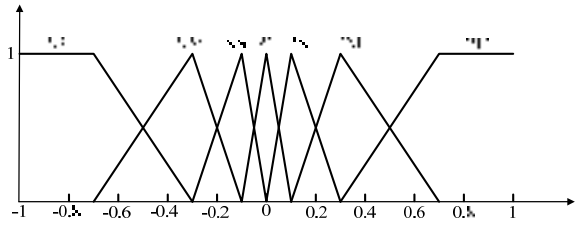

Fig. 7. Fuzzy membership functions of the proposed FLE

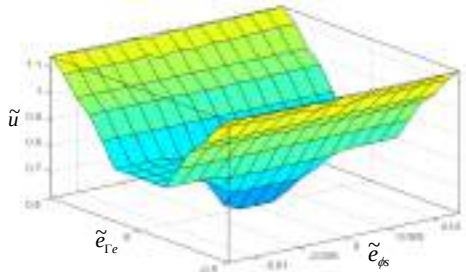

Fig. 8. Control surface of the fuzzy logic estimator

Just like the first step of fuzzification, the defuzzification module transforms the overall control output ($\tilde{u}$) obtained in the previous phase, to corresponding physical values (voltage) that system can accept. The voltage vector amplitude is then obtained by multiplying the crisp output value (d*u*), by an appropriate gain. This latter is chosen so that the maximum amplitude of the reference voltage vector should not exceed the voltage vector maximum amplitude generated by a two level PWM inverter.

Principle of Space Vector Modulation strategy. SVM technique is an advanced computation intensive PWM method and possibly the best PWM strategy for three-phase VSI used in industrial applications such as control of induction motors. Practically this modulation technique has several advantages either for inverter or motor such as; better utilization of DC-link voltage, less of torque ripples, motor current with lower Total Harmonic Distortion (THD), minimum of switching losses, and simplicity of implementation in digital systems [9, 10, 14, 23].

SVM principle is based on the concept of approximating a rotating reference voltage vector ($\overrightarrow{V_S^*}$) by using a combination of two out of the eight possible state vectors that can be generated from a three-phase VSI. This strategy differs from the sinusoidal PWM in such way that, there is no separate modulator used for each of three phases. Instead, the reference voltage vector is processed as a whole. In fact, the SVM is produced by a regular sampling of circular locus reference voltage created on the α–β plane. These voltage samples are then represented by two actives vectors, chosen from $\overrightarrow{V_1}$ to $\overrightarrow{V_6}$, that are adjacent to the reference voltage vector together with either two null vectors; $\overrightarrow{V_0}$ and $\overrightarrow{V_7}$. The respective times corresponding to these state vectors are adjusted within a sample period [9, 10, 14].

Figure 9 shows the SVM principle, where reference vector ($\overrightarrow{V_S^*}$) is sampled at time intervals fixed and equal (T_s), called «sub-cycles». The sampled value $\overrightarrow{V_S^*}(T_S)$ is then used to solve the following equations:

$$\begin{cases} T_k \cdot \overrightarrow{V_k} + T_{k+1} \cdot \overrightarrow{V}_{k+1} = T_S \cdot \overrightarrow{V_S^*}(T_S); \\ T_0 = T_7 = T_S - T_k - T_{k+1}, \end{cases} \quad (13)$$

where $\overrightarrow{V_k}$ and $\overrightarrow{V_{k+1}}$ are two switching state vectors adjacent in space, to the reference voltage vector ($\overrightarrow{V_S^*}$).

Solution of (13) gives application times of switching state vectors

$$\begin{cases} T_k = \sqrt{3}\left(\sin\left[k\cdot\frac{\pi}{3}\right]\cdot V_{s\alpha}^* - \cos\left[k\cdot\frac{\pi}{3}\right]\cdot V_{s\beta}^*\right)\cdot\frac{T_S}{V_{dc}}; \\ T_{k+1} = \sqrt{3}\left(-\sin\left[(k-1)\cdot\frac{\pi}{3}\right]\cdot V_{s\alpha}^* + \cos\left[(k-1)\cdot\frac{\pi}{3}\right]\cdot V_{s\beta}^*\right)\cdot\frac{T_S}{V_{dc}}. \end{cases} \quad (14)$$

If the over-modulation mode (T_k+T_{k+1}>T_S) occurs, state vectors application time should be scaled as (15) to generate the best approximation of the reference voltage vector. This may be detected by examining the sign of calculated T_0 and limit is then applied by maintaining the same angle for the reference voltage vector

$$\begin{cases} T'_{k,\,k+1} = T_{k,\,k+1} \cdot \dfrac{T_S}{T_k + T_{k+1}}; \\ T'_0 = T'_7 = 0. \end{cases} \quad (15)$$

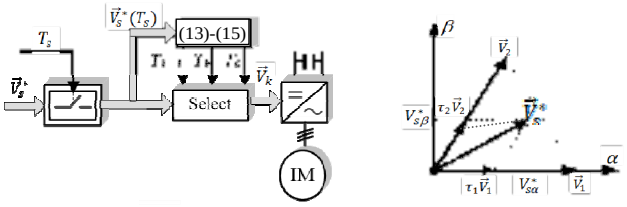

a *b*

Fig. 9. Principle of the SVM: *a* – functional diagram; *b* – switching state vectors in the first 60°–sector

Having computed these modulation times, an adequate sequence of the state vectors must be well determined. The modulation scheme, used in this work, is based on a symmetrical sequence within each sample period (Fig. 10). Thus, switching sequence applied for a given sector can be described as:

$$\overrightarrow{V_{0,7}} \Rightarrow \overrightarrow{V_k} \Rightarrow \vec{V}_{k+1} \Rightarrow \overrightarrow{V_{0,7}} \Rightarrow \vec{V}_{k+1} \Rightarrow \overrightarrow{V_k} \Rightarrow \overrightarrow{V_{0,7}}.$$

This sequence is characterized by the weakest switching losses and also the lowest harmonic distortion due to the resulted symmetry in switching pulses waveform of the inverter power components.

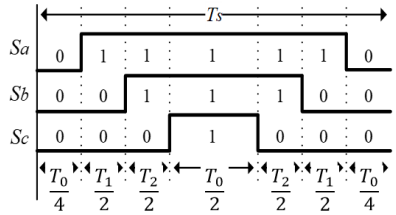

Fig. 10. Switching pulses waveform for the first 60°–sector

Modified Direct Torque Control (MDTC). The proposed MDTC structure for IM is shown in Fig. 11, where the hysteresis comparators and switching table of conventional DTC are eliminated and replaced by

- prediction of the reference stator flux;
- determination of the reference voltage space vector;
- application of the SVM technique.

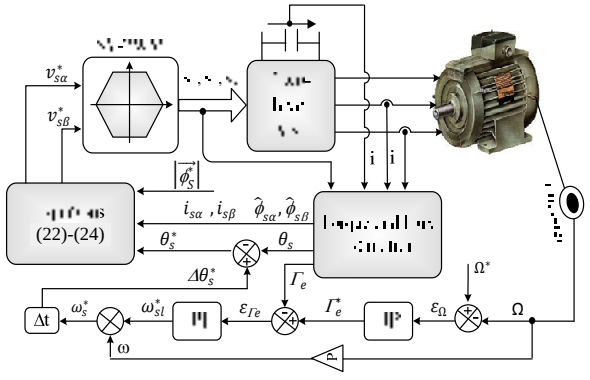

Fig. 11. Block diagram of the proposed MDTC approach

In fact, in MDTC structure, the torque control is achieved by maintaining constant amplitude for the reference stator flux. From (16) torque control is directly performed by controlling the torque angle changes (Fig. 12). This latter represents the angle between the two flux vectors (of stator and rotor). Thus, the instantaneous electromagnetic torque can be described as follows:

$$\Gamma_e = \frac{3}{2}\cdot p\cdot\frac{L_m^2}{R_r\cdot L_S^2}\cdot\left|\overrightarrow{\phi_S^*}\right|^2\cdot\left[1-e^{-t/\tau}\right]\cdot(\omega_S-\omega), \quad (16)$$

where $\tau = \sigma \cdot L_r / R_r$ is the time constant.

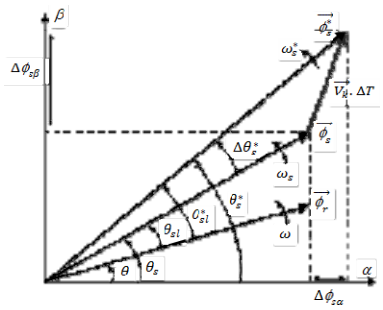

Fig. 12. Direct control of the stator flux vector

The slip angular frequency depended on the stator angular frequency (ω_S) and rotor angular frequency (ω), can be written as:

$$\omega_{Sl} = \omega_S - \omega\,, \quad (17)$$

or

$$\omega_{Sl} = \frac{\mathrm{d}\theta_{Sl}}{\mathrm{d}t} \approx \frac{\Delta\theta_{Sl}}{\Delta t}\,, \quad (18)$$

where θ_{Sl} is the angle between the two flux vectors and Δt is the sampling time.

By substituting (18) in (16), the instantaneous electromagnetic torque is given by:

$$\Gamma_e = \frac{3}{2}\cdot p\cdot\frac{L_m^2}{R_r\cdot L_S^2}\cdot\left|\overrightarrow{\phi_S^*}\right|^2\cdot\left[1-e^{-t/\tau}\right]\cdot\left(\frac{\Delta\theta_{Sl}}{\Delta t}\right). \quad (19)$$

According to (19), the control of the instantaneous electromagnetic torque is achieved by changing the value of slip angle that is controlled by using a direct control method for the stator flux vector. On the other hand, the reference torque is generated from the speed IP controller. Therefore, quantity $\varepsilon_{\Gamma e}$ is the obtained error between the reference torque and estimated or real torque (Fig. 11). In order to compensate this error, the angle of stator flux (θ_S) must be increased using the following expression (where ω_{Sl}^* is the slip angle that is generated from the torque PI controller)

$$\theta_S^* = \theta_S + \Delta\theta_S^* = \theta_S + \left(\omega_{Sl}^* + \omega\right)\cdot\Delta t\,. \quad (20)$$

Therefore, the required reference stator flux vector will be given in a polar form by:

$$\overrightarrow{\phi_S^*} = \left|\overrightarrow{\phi_S^*}\right|\angle\theta_s^*\,, \quad (21)$$

where $|\overrightarrow{\phi_S^*}|$ is maintained constant at its rated value.

The reference stator flux components and corresponding flux errors are given respectively by:

$$\begin{cases}\phi_{S\alpha}^* = \left|\overrightarrow{\phi_S^*}\right|\cdot\cos\theta_s^* \\ \phi_{S\beta}^* = \left|\overrightarrow{\phi_S^*}\right|\cdot\sin\theta_s^*\end{cases}, \quad (22)$$

$$\begin{cases}\Delta\phi_{S\alpha} = \phi_{S\alpha}^* - \hat{\phi}_{S\alpha} \\ \Delta\phi_{S\beta} = \phi_{S\beta}^* - \hat{\phi}_{S\beta}\end{cases}, \quad (23)$$

Then the reference stator voltage vector components are given by the following expressions:

$$\begin{cases}v_{S\alpha}^* = R_S\cdot i_{S\alpha} + \dfrac{\Delta\phi_{S\alpha}}{\Delta t} \\ v_{S\beta}^* = R_S\cdot i_{S\beta} + \dfrac{\Delta\phi_{S\beta}}{\Delta t}\end{cases}, \quad (24)$$

Subsequently, by using these reference voltage components, the inverter control signals will be designed in such way that the average space vector generated within sample period is equal to the sampled value of the reference stator voltage vector.

Simulation results and discussion. To show the effectiveness of the two proposed DTC-SVM structures, the simulation work is carried out, on an IM, using the Matlab/Simulink software and/or fuzzy logic tools. The parameters of used motor are listed in Table 4.

Table 4

Induction motor parameters

Parameters	Values
Rated power, kW	4
Stator voltage, V	220
Stator resistance, Ω	1.2
Rotor resistance, Ω	1.8
Stator cyclic inductance, H	0.1554
Rotor cyclic inductance, H	0.1568
Mutual inductance, H	0.15
Number of pairs of poles	2
Inertia, N·m/rad·s	0.07
Friction coefficient, kg·m^2	0.0001

In order to validate these two approaches of DTC-SVM, their performances are compared, under the same conditions, with those of classical DTC. In turn, the

dynamic behaviour of these three DTC structures (with speed IP controller) is tested under high and low speed and with various load torque commands. Simulation results, included in Fig. 13, show that a good tracking performances can still be achieved in the responses of speed, torque, flux and current with no distinct difference among the three DTC approaches (for all tested cases in terms of the damping capability and transient response under different reference speeds and mechanical loads).

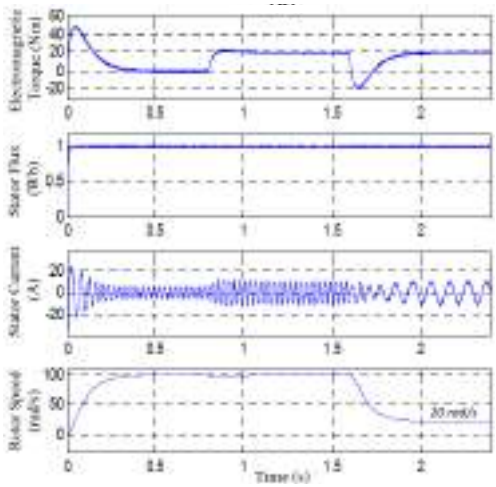

a

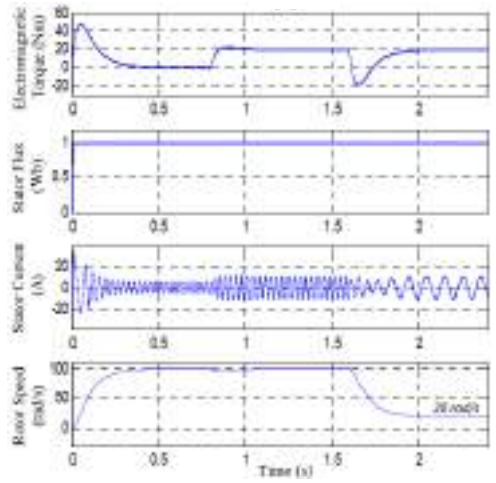

b

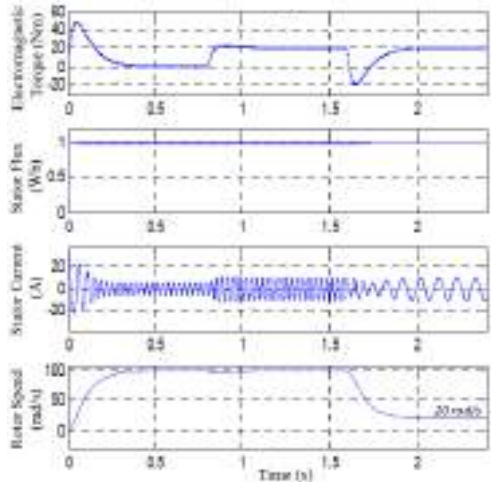

c

Fig. 13. System responses for various operating conditions: *a* – classical DTC; *b* – DFTC; *c* –MDTC

For a close inspection of the steady-state performances, we give in Fig. 14, 15 the static responses of the three DTC structures. Where for all, the machine is operating at high speed (100 rad/s) and with full load (20 N·m). From these results, it is possible to see that the two DTC-SVM approaches illustrate some better performances by reducing the ripples in the torque and stator flux and attenuating the speed vibrations.

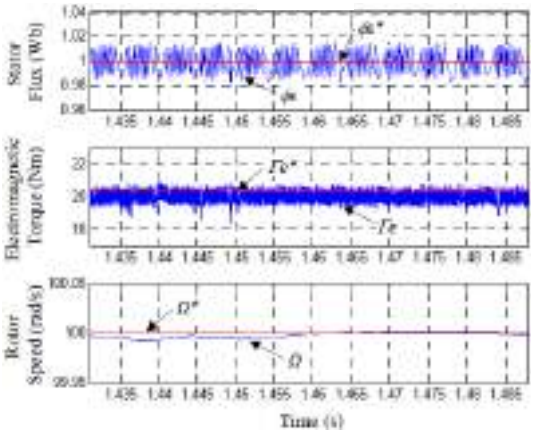

a

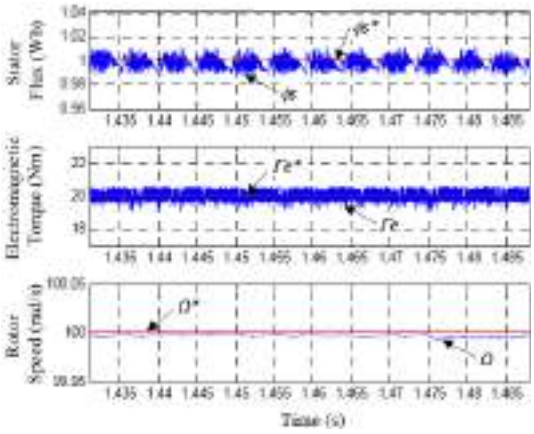

b

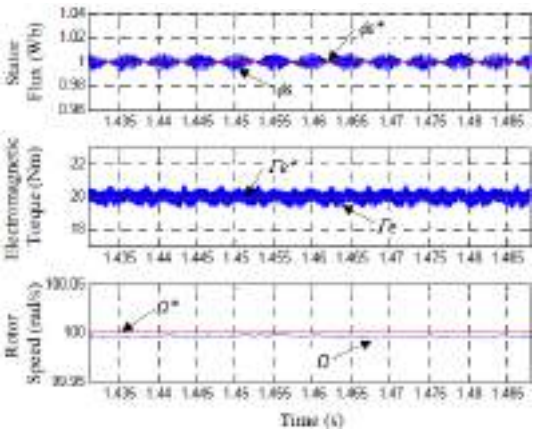

c

Fig. 14. Steady-state responses of stator flux, torque and speed: *a* – classical DTC; *b* – DFTC; *c* – MDTC

For the same steady-state operating conditions, we see significantly in Fig. 15 that the harmonic content of the stator current is quite attenuated by employing mainly the MDTC structure, wherein the stator line voltage is found closer to the desired staircase form.

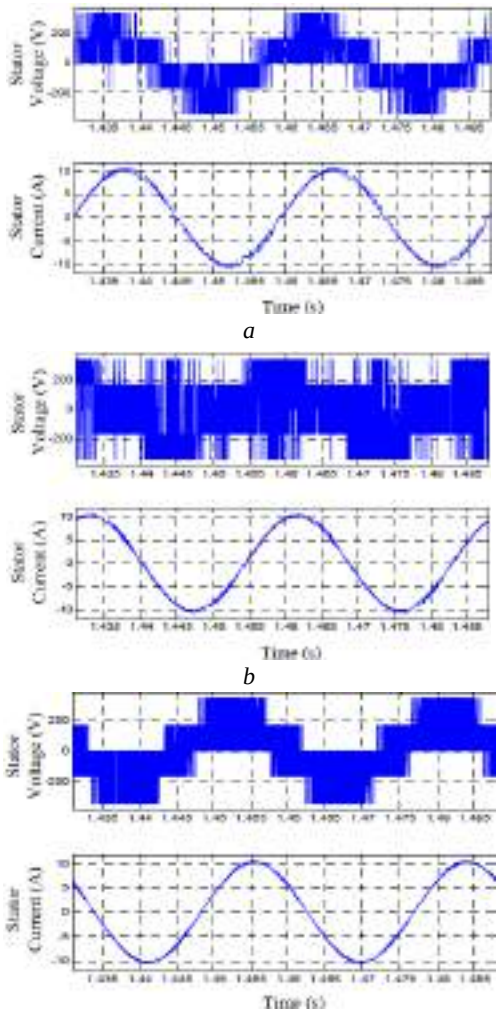

Fig. 15. Static responses of stator voltages and currents: *a* – Classical DTC; *b* – DFTC; *c* – MDTC

Moreover, from the trajectories of the stator flux given in Fig. 16, we can notice an appreciable reduction in stator flux ripples, which is obtained with the two DTC-SVM structures. Particularly using the MDTC approach, the stator flux path represents the fastest dynamic response with the lowest ripples.

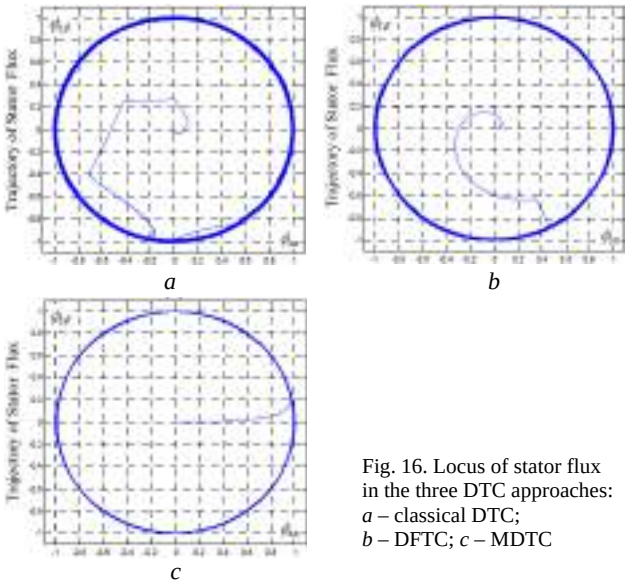

Fig. 16. Locus of stator flux in the three DTC approaches: *a* – classical DTC; *b* – DFTC; *c* – MDTC

By representing the inverter switching frequency in Fig. 17, we have demonstrated that the use of SVM strategy in MDTC structure gives in reality a fixed switching frequency and equalling the sample frequency (5 kHz) used in the modulation sequence of stator voltage space vector. On the other hand, we have verified that with DFTC structure the switching frequency has a fixed average value for various speed or torque references.

Therefore, from this analysis we have shown that the two proposed structures of DTC-SVM exhibit good static and dynamic performances with low torque ripples and a fixed switching frequency (over a wide range of torque or speed control). All of these benefits are obtained through the use of the SVM strategy and the speed IP controller.

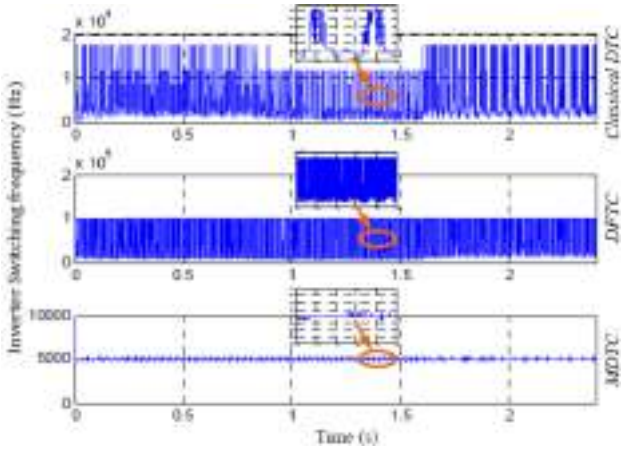

Fig. 17. Inverter switching frequency in each DTC approach

Conclusions.

The study of the two proposed direct torque control approaches (with space vector modulation), applied to the induction motor drive, is carried out here by means of physical considerations, analytical developments and simulation tests. Thus demonstrating how the electromagnetic torque and the stator flux can be kept under control through the application of the space vector modulation strategy.

A comparison between the classical direct torque control and the two direct torque control structures (with space vector modulation) is presented where the modification aim was some drawbacks attenuation of conventional direct torque control such as; the torque ripples, current distortion and random switching frequency variation. Indeed, the two proposed direct torque control approaches (with speed IP controller) have shown, through the different simulation tests, their effectiveness and superiority over the classical direct torque control without deteriorating the dynamic control capability of this technique.

The foremost revealed improvements of these two approaches are:

- ripples reduction in the torque and stator flux for either static or dynamic responses (under high and low speed operation);
- more attenuated distortion in the stator voltage and current waveforms by using the modified direct torque control structure;
- a switching frequency with fixed average value is achieved under various operating conditions (thanks to use of the space vector modulation strategy);
- fast dynamic response for the stator flux and a constant switching frequency in the inverter by using particularly the modified direct torque control structure.

In fact, the lowest switching frequency is obtained with the modified direct torque control approach. That will reduce the switching losses as well as stress on the inverter semiconductor components. Also, the modified direct torque control structure is more suitable for real time implementation due to its efficiency and simplicity.

Conflict of interest. The author declares that he has no conflicts of interest.

REFERENCES

1. Naganathan P., Srinivas S. Direct Torque Control Techniques of Three-Level H-Bridge Inverter Fed Induction Motor for Torque Ripple Reduction at Low Speed Operations. *IEEE Transactions on Industrial Electronics*, 2020, vol. 67, no. 10, pp. 8262-8270. doi: https://doi.org/10.1109/TIE.2019.2950840.

2. Djagarov N., Milushev H., Kononov Y., Djagarova J. Adaptive Controller for Induction Machine Direct Torque Control. *2021 17th Conference on Electrical Machines, Drives and Power Systems (ELMA)*, 2021, pp. 1-4. doi: https://doi.org/10.1109/ELMA52514.2021.9503085.

3. Ravi H.K., Chokkalingam L.N. Three Dimensional Switching Table for Reducing Torque Ripple and Switching Frequency in Direct Torque Controlled Induction Motor Drives. *2021 IEEE 12th Energy Conversion Congress & Exposition - Asia (ECCE-Asia)*, 2021, pp. 1515-1519. doi: https://doi.org/10.1109/ECCE-Asia49820.2021.9479266.

4. Moussaoui L. Direct torque control for a three-level NPC voltage source inverter fed induction motor drive. *International Conference on Electrical Engineering and Automatic Control*. Setif, Algeria, 2013.

5. Viet N.H., Paraschiv N. An Investigation on Twelve Sectors Direct Torque Control for Induction Motors fed by Matrix Converter. *2020 12th International Conference on Electronics, Computers and Artificial Intelligence (ECAI)*, 2020, pp. 1-5. doi: https://doi.org/10.1109/ECAI50035.2020.9223148.

6. Singh P., Gaur P., Mittal A.P. Improved Direct Torque Control Scheme based on Modified Torque Hysteresis Band. *2020 IEEE 5th International Conference on Computing Communication and Automation (ICCCA)*, 2020, pp. 725-729. doi: https://doi.org/10.1109/ICCCA49541.2020.9250910.

7. Koratkar P.J., Sabnis A. Comparative analysis of different control approaches of direct torque control induction motor drive. *2017 International Conference on Intelligent Computing, Instrumentation and Control Technologies (ICICICT)*, 2017, pp. 831-835. doi: https://doi.org/10.1109/ICICICT1.2017.8342672.

8. Pal A., Srivastava G.D., Kulkarni R.D. Simulation of Sensorless Speed Control of Induction Motor Using Direct Torque Control Technique Employing Five Level Torque Comparator and Twelve Sector Method. *2019 International Conference on Nascent Technologies in Engineering (ICNTE)*, 2019, pp. 1-6. doi: https://doi.org/10.1109/ICNTE44896.2019.8945936.

9. Moussaoui L., Moussi A. An open loop space vector PWM control for CSI-fed field-oriented induction motor drive with improved performances and reduced pulsating torque. *WSEAS Transactions on Circuits and Systems*, 2005, vol. 4, no. 2, pp. 71-77.

10. Moussaoui L., Moussi A. Performances improvement and torque ripple mitigation for CSI-fed vector controlled induction motor based on space vector PWM control. *Journal of Electrical Engineering*, 2005, vol. 5, no. 1, pp. 5-12.

11. Malyar V.S., Hamola O.Y., Maday V.S. Modelling of dynamic modes of an induction electric drive at periodic load. *Electrical Engineering & Electromechanics*, 2020, no. 3, pp. 9-14. doi: https://doi.org/10.20998/2074-272X.2020.3.02.

12. Petrushin V.S., Bielikova L.Y., Plotkin Y.R., Yenoktaiev R.N. Comparison of adjustable high-phase order induction motors' merits. *Electrical Engineering & Electromechanics*, 2016, no. 1, pp. 38-41. doi: https://doi.org/10.20998/2074-272X.2016.1.07.

13. Lobov V.I., Lobova K.V. The thyristor converter influence on the pulsations of the electromagnetic torque of the induction motor at parametrical control. *Electrical Engineering & Electromechanics*, 2017, no. 4, pp. 34-41. doi: https://doi.org/10.20998/2074-272X.2017.4.06.

14. Setiana H., Husnayain F., Yusivar F. Speed Sensorless Control of Dual Induction Motor using Direct Torque Control - Space Vector Modulation. *2019 IEEE 2nd International Conference on Power and Energy Applications (ICPEA)*, 2019, pp. 110-114. doi: https://doi.org/10.1109/ICPEA.2019.8818504.

15. Dehigolle Gedara A., Ekneligoda N.C. Direct torque control of induction motor using sliding-mode and fuzzy-logic methods. *2018 IEEE Power & Energy Society Innovative Smart Grid Technologies Conference (ISGT)*, 2018, pp. 1-5. doi: https://doi.org/10.1109/ISGT.2018.8403326.

16. Rosic M.M., Bebic M.Z. Analysis of torque ripple reduction in induction motor DTC drive with multiple voltage vectors. *Advances in Electrical and Computer Engineering*, 2015, vol. 15, no. 1, pp. 105-114. doi: https://doi.org/10.4316/AECE.2015.01015.

17. Lunardi A.S., Sguarezi A.J., Filho. Experimental results for predictive direct torque control for a squirrel cage induction motor. *2017 Brazilian Power Electronics Conference (COBEP)*, 2017, pp. 1-5. doi: https://doi.org/10.1109/COBEP.2017.8257222.

18. Manuprasad P., Mohanty K.B. Implementation of 12 Sector Fuzzy Controller for Direct Torque Control of Induction Motor. *2019 Innovations in Power and Advanced Computing Technologies (i-PACT)*, 2019, pp. 1-6. doi: https://doi.org/10.1109/i-PACT44901.2019.8960096.

19. Yu C., Wang H., Sung G., Huang H. Modified Direct Torque Control Application-Specific Integrated Circuit with Five-Stage Fuzzy Hysteresis and a Proportional–Integral–Derivative Controller for a Three-Phase Induction Motor. *2018 IEEE International Conference on Systems, Man, and Cybernetics (SMC)*, 2018, pp. 2413-2417. doi: https://doi.org/10.1109/SMC.2018.00414.

20. Wu X., Huang W., Lin X. A Novel Direct Torque Control with or without Duty Ratio Optimization for Induction Motors. *2019 22nd International Conference on Electrical Machines and Systems (ICEMS)*, 2019, pp. 1-4. doi: https://doi.org/10.1109/ICEMS.2019.8922455.

21. Venkataramana Naik N., Singh S.P. A Novel Interval Type-2 Fuzzy-Based Direct Torque Control of Induction Motor Drive Using Five-Level Diode-Clamped Inverter. *IEEE Transactions on Industrial Electronics*, 2021, vol. 68, no. 1, pp. 149-159. doi: https://doi.org/10.1109/TIE.2019.2960738.

22. Moussaoui L. Study and simulation of a fuzzy-controlled shunt active power filter using two different control algorithms. *1st International Conference on Electrical Engineering*, Biskra, Algeria, 2014.

23. Wu X., Huang W., Lin X., Zhu S. An Initial Trial to Drive Induction Motors by Synchronized SVPWM-Based Direct Torque Control. *2020 IEEE 9th International Power Electronics and Motion Control Conference (IPEMC2020-ECCE Asia)*, 2020, pp. 342-345. doi: https://doi.org/10.1109/IPEMC-ECCEAsia48364.2020.9368145.

Received 03.11.2021
Accepted 16.12.2021
Published 23.02.2022

Leila Moussaoui, Doctor of Electrical Engineering,
Department of Electrical Engineering, Faculty of Technology,
Ferhat Abbas Setif 1 University,
Cité Maabouda, Route de Bejaia, Setif, 19000, Algeria,
e-mail: ufas.lmoussaoui@gmail.com (Corresponding author)